RECENT CMS RESULTS ON INELASTIC CROSS-SECTION MEASUREMENTS*

Sercan Sen

on behalf of the CMS Collaboration

Department of Physics Engineering, Hacettepe University, Ankara, Turkey

(Received March 5, 2019)

A measurement of the inelastic proton–proton (pp) cross section is presented. The analysis is based on the data collected in 2015 at a center-of-mass energy of 13 TeV with the CMS detector at the LHC. The inelastic pp cross section is measured in two fiducial ranges and the results are compared to the predictions of various models.

DOI:10.5506/APhysPolBSupp.12.753

1. Introduction

The inelastic proton–proton cross section is a fundamental observable both in hadron collider physics and in particle astrophysics. The experiments at the LHC have measured the inelastic cross section in pp collisions in the same or in different phase spaces and at various center-of-mass energies so far. However, large modeling uncertainties are observed when extrapolating the results to the full phase space and/or to the higher center-of-mass energies. Further measurements, especially in unexplored regions of the phase space, are, therefore, essential to constrain the phenomenological models.

These proceedings report on the measurement of inelastic pp cross section at $\sqrt{s} = 13\,\text{TeV}$ performed with the data collected by the CMS detector at the LHC [1]. A detailed description of the CMS detector can be found in Ref. [2]. The inelastic pp cross section is measured in two fiducial ranges defined by the acceptance of the forward calorimeters, HF and CASTOR, covering the pseudorapidities of $3 < |\eta| < 5.2$ and $-6.6 < \eta < -5.2$, respectively. The inclusion of the CASTOR calorimeter in the analysis provides a broader coverage of pseudorapidity and thus allows to measure an inelastic

* Presented at the Diffraction and Low-x 2018 Workshop, August 26–September 1, 2018, Reggio Calabria, Italy.

cross section in an extended phase space defined by $M_X > 4.1$ GeV and $M_Y > 13$ GeV, where M_X and M_Y are the invariant masses of the two hadronic systems separated by the largest rapidity gap in the event.

2. Event selection and reconstruction

The low pile-up *pp* collision data used in this analysis were collected with the CMS detector at two different magnetic field strengths ($B = 0\,\mathrm{T}$ and $B = 3.8\,\mathrm{T}$) in 2015 at a center-of-mass energy $\sqrt{s} = 13\,\mathrm{TeV}$. The total integrated luminosity corresponds to 40.8 $\mu\mathrm{b}^{-1}$ (28.0 $\mu\mathrm{b}^{-1}$) for $B = 3.8\,\mathrm{T}$ ($B = 0\,\mathrm{T}$) samples. The CASTOR calorimeter was included in the data taking only for the runs at $B = 0\,\mathrm{T}$.

The events were triggered based on BPTX (The Beam Pickup Timing for the eXperiment) signals, requiring the presence of both beams in the interaction point ("ZeroBias") or requiring the presence of only one beam ("SingleBunch") or no beams ("EmptyBunch"). The SingleBunch and EmptyBunch data were used to study the backgrounds such as beam–gas interactions and electronic noise.

The following event selections are applied to select inelastic events offline in two detector acceptances:

(i) HF-OR: requires an energy deposition greater than 5 GeV in any of the two HF calorimeters,

(ii) HF-OR-CASTOR: requires energy deposition greater than 5 GeV either in any of the two HF calorimeters or in CASTOR.

The calorimeter thresholds were optimized by studying the noise without beam. The number of selected inelastic events is first corrected for the remaining noise contributions as the following:

$$N_{\mathrm{cor}} = N_{\mathrm{ZB}}[(F_{\mathrm{ZB}} - F_{\mathrm{EB}}) + F_{\mathrm{EB}}(F_{\mathrm{ZB}} - F_{\mathrm{EB}})]\,, \tag{2.1}$$

where N_{ZB} corresponds to the number of ZeroBias triggered events and F_{ZB} (F_{EB}) is the fraction of ZeroBias (EmptyBunch) triggered events that pass the event selection criteria.

A data-driven method is used to correct for the effect of pileup. The number of visible *pp* interactions per bunch crossing, n, follows a Poisson statistics, $P(n, \lambda)$, with mean value λ. The probability to have no interaction in a filled bunch is given by $P(0, \lambda) \equiv \exp(-\lambda) = 1 - N_{\mathrm{cor}}/N_{\mathrm{ZB}}$. This makes it possible to determine the mean number of *pp* interactions per bunch crossing, $\lambda = -\ln(1 - N_{\mathrm{cor}}/N_{\mathrm{ZB}})$, and further correct the inelastic event count using the following pileup correction factor:

$$f_{\mathrm{PU}} = \frac{\sum_{n=0}^{\infty} nP(n,\lambda)}{\sum_{n=1}^{\infty} P(n,\lambda)} = \frac{\lambda}{1 - P(0,\lambda)}\,. \tag{2.2}$$

The total reconstructed number of interactions, corrected for the contributions of noise and pileup, is then given by

$$N_{\rm int} = \sum_{\rm bunches} N^{\rm b}_{\rm cor}\, f^{\rm b}_{\rm PU}\,, \tag{2.3}$$

where $N^{\rm b}_{\rm cor}$ is the number of noise-corrected events and $f^{\rm b}_{\rm PU}$ is the pileup correction factors calculated for individual bunches.

3. Extraction of the fiducial cross section

The measured number of inelastic interactions is corrected to the stable-particle level in order to take into account detector efficiencies and resolutions. The phase space in stable-particle level is defined based on ξ. First, the largest rapidity gap is reconstructed in the full phase-space domain, and the final-state particles are divided into two subsystems, X (negative side) and Y (positive side), separated by the largest rapidity gap in the event. Then, the invariant mass ($M_{\rm X(Y)}$) of each subsystem is calculated, and $\xi_{\rm X}$ and $\xi_{\rm Y}$ are obtained as follows:

$$\xi_{\rm X} = \frac{M^2_{\rm X}}{s}\,, \qquad \xi_{\rm Y} = \frac{M^2_{\rm Y}}{s}\,, \tag{3.1}$$

where s is the center-of-mass energy. In addition, ξ is defined as the maximum of $\xi_{\rm X}$ and $\xi_{\rm Y}$. In order to closely match the stable-particle level phase-space definition and the offline detector-level selection, the limits on $\xi_{\rm X}$ and $\xi_{\rm Y}$ are optimized by studying the efficiency (ϵ_ξ) and contamination (b_ξ) factors using fully simulated events from various Monte Carlo event generators.

The optimal acceptance is determined as $\xi > 10^{-6}$ for HF-OR detector-level selection, and $\xi_{\rm X} > 10^{-7}$ or $\xi_{\rm Y} > 10^{-6}$ for HF-OR-CASTOR detector-level selection. Note that the CASTOR calorimeter, which is installed only at minus side, allows a larger coverage of the phase space and, therefore, a lower limit on $\xi_{\rm X}$.

Taking into account the efficiency and contamination factors and the normalization to the integrated luminosity ($\mathcal{L}$), the final fiducial cross section is calculated as

$$\sigma = \frac{N_{\rm int}\,(1 - b_\xi)}{\epsilon_\xi\,\mathcal{L}}\,, \tag{3.2}$$

where $N_{\rm int}$ is the number of interactions corrected for noise and pileup. The results are given in Table I.

The systematic uncertainties from different sources, such as model dependence, energy scale uncertainties of HF and CASTOR calorimeters, and run-to-run variation of the measured cross sections are estimated and their contributions to the systematic uncertainty in the cross-section measurement are summarized in Table II.

TABLE I

The noise-subtracted fraction of events ($N_{\rm cor}/(N_{\rm ZB} \times F_{\rm ZB})$), average pileup ($\lambda$), and fiducial cross section for each run used in the analysis. The errors given for fiducial cross section represent the statistical uncertainty only.

Runs $B = 3.8\,\mathrm{T}$	$N_{\rm cor}/(N_{\rm ZB} \times F_{\rm ZB})$ [%]	λ	Fiducial cross section [mb] $\xi > 10^{-6}$
254989	98.5	0.52	67.35 ± 0.05
255019	99.9	0.54	67.66 ± 0.04
255029	99.3	0.54	67.50 ± 0.04
Runs $B = 0\,\mathrm{T}$	**$N_{\rm cor}/(N_{\rm ZB} \times F_{\rm ZB})$ [%]**	**λ**	**Fiducial cross section [mb] $\xi_{\rm X} > 10^{-7}$ or $\xi_{\rm Y} > 10^{-6}$**
247324	98.5	0.05	68.88 ± 0.49
247920	98.9	0.34	68.63 ± 0.08
247934	98.8	0.32	68.63 ± 0.09

TABLE II

Contributions to the systematic uncertainties in the cross sections measured in two phase-space regions.

	$\sigma(\xi > 10^{-6})$ [mb]	$\sigma(\xi_{\rm X} > 10^{-7}$ or $\xi_{\rm Y} > 10^{-6})$ [mb]
Model dependence	0.68	0.39
HF energy scale	0.35	0.14
CASTOR energy scale	—	0.04
Run-to-run variation	0.15	0.14
Total	0.78	0.45
Integrated luminosity	1.55	1.58

4. Results and summary

The fiducial cross sections for all runs used in the analysis are presented in Table I. The final value of the fiducial cross section measured with the HF calorimeters only is determined by taking the average of the results at $B = 3.8\,\mathrm{T}$ and it is found to be

$$\sigma\left(\xi > 10^{-6}\right) = 67.5 \pm 0.8\ (\mathrm{syst.}) \pm 1.6\ (\mathrm{lumi.})\ \mathrm{mb}\,, \tag{4.1}$$

where the statistical uncertainty is negligible. This result is in agreement, within uncertainties, with the cross section measured by ATLAS, $\sigma(\xi > 10^{-6}) = 68.1 \pm 0.6$ (syst.) ± 1.3 (lumi.) mb [6], in the same phase-space domain.

Likewise, the fiducial cross section in the enlarged phase space is obtained by taking the average of the cross sections measured with the HF and CASTOR calorimeters and it is found as

$$\sigma\left(\xi_{\mathrm{X}} > 10^{-7} \text{ or } \xi_{\mathrm{Y}} > 10^{-6}\right) = 68.6 \pm 0.5 \text{ (syst.)} \pm 1.6 \text{ (lumi.) mb}\,. \quad (4.2)$$

In Fig. 1, the measurements are compared to the predictions of different models that are widely used to simulate high-energy hadron–hadron interactions. Most models overestimate the data in both measurement ranges. The PYTHIA 8 Monash [3, 4] MC generator with DL (Donnachie–Landshoff) parameterization [5] has the best description of the data for $\xi > 10^{-6}$ but it overestimates the data for $\xi_{\mathrm{X}} > 10^{-7}$ or $\xi_{\mathrm{Y}} > 10^{-6}$, which means that it predicts a too large increase in the cross section when going from forward to very forward rapidities.

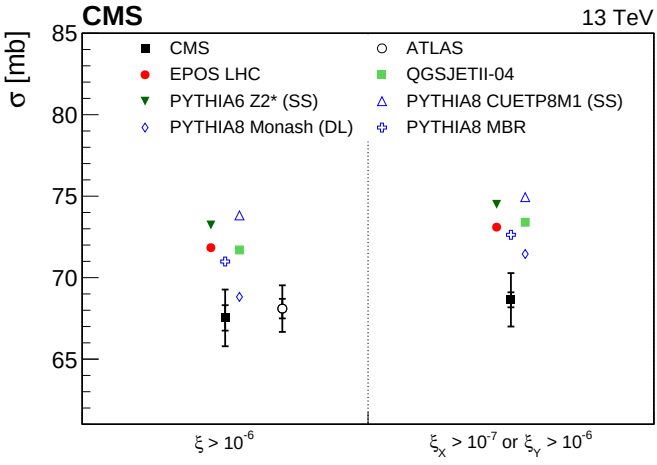

Fig. 1. Proton–proton inelastic cross section at a center-of-mass energy $\sqrt{s} = 13\,\mathrm{TeV}$ measured by CMS in two phase-space regions [1]. The results are compared to the predictions of Monte Carlo generators and to the ATLAS result.

The relative increase in the cross section from $\xi > 10^{-6}$ to $\xi_{\mathrm{X}} > 10^{-7}$ or $\xi_{\mathrm{Y}} > 10^{-6}$ observed in the data is presented in Table III together with the predictions of the models. The relative increase in the cross section is described reasonably well by most models, but none of the models simultaneously describe the absolute cross sections and relative increase. In addition, the same models generally describe the inelastic *pp* cross section

well in the full phase-space domain [6, 7], while overestimating the fiducial cross sections. This indicates that the "missing part" of the cross section, which is dominated by the contribution from low mass diffractive processes, is underestimated by the models.

TABLE III

The increase in the cross section from $\xi > 10^{-6}$ to $\xi_X > 10^{-7}$ or $\xi_Y > 10^{-6}$ presented as percentages for the data and various models.

	Relative cross-section increase in %
Data	1.64 ± 0.53
EPOS LHC	1.76
QGSJetII-04	2.36
PYTHIA 6 Z2* (SS)	1.74
PYTHIA 8 CUETP8M1 (SS)	1.52
PYTHIA 8 Monash (DL)	3.83
PYTHIA 8 MBR	2.32

This work was supported by the Hacettepe University (Turkey) Scientific Research Projects Program through the project: FBB-2017-15425.

REFERENCES

[1] CMS Collaboration, *J. High Energy Phys.* **1807**, 161 (2018).
[2] CMS Collaboration, *JINST* **3**, S08004 (2008).
[3] T. Sjöstrand, S. Mrenna, P. Skands, *Comput. Phys. Commun.* **178**, 852 (2008).
[4] P. Skands, S. Carrazza, J. Rojo, *Eur. Phys. J. C* **74**, 3024 (2014).
[5] A. Donnachie, P.V. Landshoff, *Phys. Lett. B* **296**, 227 (1992).
[6] ATLAS Collaboration, *Phys. Rev. Lett.* **117**, 182002 (2016).
[7] TOTEM Collaboration, `arXiv:1712.06153 [hep-ex]`.